Electrical Impedance Spectra to Monitor Damage during Tensile Loading of Cement Composites

by

Alva Peled
Center for Advanced Cement-Based Materials
Northwestern University
Evanston, Illinois USA

Josep M. Torrents
Technical University of Catalonia (UPC)
Barcelona, Spain

Thomas O. Mason, Surendra P. Shah
Center for Advanced Cement-Based Materials
Northwestern University
Evanston, Illinois USA

and

Edward J. Garboczi
Building and Fire Research Laboratory
National Institute of Standards and Technology
Gaithersburg, MD 20899 USA

Reprinted from ACI Materials Journal, Vol. 98, No. 4, 313-322, July-August 2001.

NIST
National Institute of Standards and Technology
Technology Administration, U.S. Department of Commerce

ACI MATERIALS JOURNAL TECHNICAL PAPER

Title no. 98-M34

Electrical Impedance Spectra to Monitor Damage during Tensile Loading of Cement Composites

by Alva Peled, Josep M. Torrents, Thomas O. Mason, Surendra P. Shah, and Edward J. Garboczi

Conductive fibers can reinforce concrete and monitor damage leading to the development of smart material. This work studied the correlation between the electrical (DC and AC) and mechanical properties of cement composites reinforced with conductive carbon fibers. The tensile behavior and impedance behavior of extruded and notched composites with a fiber volume fraction of 0.5 and 3% were examined; mechanical load and electrical field were applied longitudinally (in the direction of extrusion). The crack growth of these composites during loading was observed and analyzed by digital image correlation (DIC). A good correlation between the electrical and mechanical properties was found, in that when a sudden growth in the crack was observed, a dramatic change was also noticed in the impedance values. Taking advantage of the special frequency-dependent electrical properties of conductive fiber-reinforced composites, impedance values measured during the fracture process were used to distinguish and calculate three different areas at the crack front: uncracked area, bridging area, and open area. The bridging area is the zone where the fibers bridge the propagating crack. A greater bridging area was found for the 0.5% fiber composite, compared to the 3% fiber composite. This can be explained based on differences in the final length of the carbon fibers in the two composites.

Keywords: carbon fibers; cement; composite; electrical properties; impedance spectroscopy.

RESEARCH SIGNIFICANCE

Carbon or steel fibers can be added to a cement matrix to produce a conductive composite. The mechanical status of the cement composite can affect the electrical properties (DC resistance and AC impedance) of the composite. Measurements of these electrical properties can be used as indirect nondestructive tests for cement composites, making possible the detection of damage with only the use of simple and inexpensive electrical equipment. This work established the correlation between electrical (DC and AC) and mechanical properties of cement composites reinforced with conductive carbon fibers. Using the frequency-dependent electrical properties of conductive fiber-reinforced composites, impedance values measured during the fracture process were used to distinguish and calculate three different areas at the crack front: uncracked area, bridging area, and open area.

INTRODUCTION

Fibers are added to the brittle cement matrix to control cracking and to provide ductility and improved impact resistance, thus increasing the tensile and flexural strengths of the cement matrix.[1] The reinforcing effect of short carbon fibers in a cement composite is quite high. Marked improvements in flexural strength and postcracking behavior has been reported using these fibers.[2,3] Because carbon fibers are also conductive, they can also have a strong effect on the electrical properties (DC resistance and AC impedance) of the cement composite. Such electrical measurements can be used as indirect nondestructive tests for cement composites that have been reinforced with fibers that are highly conducting compared to the cement matrix. This capability is based on the assumption that the volume electrical resistivitiy of the composite depends on crack generation and propagation under stress. Several researchers have suggested[4-6] that electrical properties can be used for nondestructive monitoring of concrete structures, making possible the detection of damage with only the use of simple and inexpensive electrical equipment.

Recently, the combined use of impedance spectroscopy (IS) and computer simulation showed that the presence of highly conductive oriented fibers in a relatively poorly conducting matrix induces changes in the impedance spectrum that can be quantitatively associated with fiber length, orientation, and volume fraction.[7,8] The main effect was that the resistance at DC or low frequency AC depended almost entirely on the matrix, while the resistance at high frequencies depended almost solely on the fiber properties and geometry.

The present work uses this frequency-dependent separation of fiber and matrix behavior to study the crack propagation process in fiber-reinforced cement composites. The tensile behavior and the impedance behavior of notched extruded cement composites reinforced with fiber volume fractions of 3 and 0.5% were studied. The crack growth of these composites during loading was observed and analyzed by digital image correlation (DIC). IS measurements were made under loaded and unloaded conditions to address the effect of specimen geometry, the manufacturing process, and the effect of fiber volume fraction. Using these IS measurements, along with numerical computation, the bridging area of the fibers could be extracted quantitatively from the tensile measurements. It is shown that such methods can be useful to elucidate the role of the reinforcing fibers during fracture.

EXPERIMENTAL DETAILS

Specimen preparation

It has been shown that extrusion process can significantly enhance the performance of fiber-reinforced cement composites.[9] A small-scale ram-type extruder was used to produce the specimens, extruding at a rate of 1.2 mm/min. In a ram extruder, a piston is used to apply pressure to the material in the barrel, to force it through a die. The pressure versus the piston displacement during the extrusion process was recorded to study the rheological properties of the fresh mixtures.[10]

ACI Materials Journal, V. 98, No. 4, July-August 2001.
MS No. 00-190 received August 11, 2000, and reviewed under Institute publication policies. Pertinent discussion will be published in the May-June 2002 *ACI Materials Journal* if received by February 1, 2002.

Alva Peled *is a post-doctoral fellow at the Center for Advanced Cement-Based Materials at Northwestern University, Evanston, Ill. She received her BTech in textile technology from Shenkar College, Israel, her MSc in chemistry of polymers and textile from the Hebrew University Israel, and her DSc degree in civil engineering from the Technion, Israel Technology Institute. Her research interests include fibers and fabrics as reinforcement for composites, processing, fiber-matrix interfaces, and microstructure.*

Josep M. Torrents *is a member of the Electronic Engineering Department, Technical University of Catalonia (UPC), Barcelona, Spain. He received his MS and PhD in telecommunication engineering from UPC in 1989 and 1996, respectively. His research interests include soil moisture determination, paste cement studies, oil characterization by electrical impedance measurement and spectroscopy, and electronic instrumentation error analysis.*

Thomas O. Mason *is a professor of Materials Science and Engineering at Northwestern University. He received his BS in ceramic science from the Pennsylvania State University, University Park, Pa., and his PhD in materials science and engineering from the Massachusetts Institute of Technology, Cambridge, Ma. His research interests include the microstructure, defect structure, and transport properties of ceramics, including cements and composites.*

Surendra P. Shah, *FACI, is a Walter P. Murphy Professor of Civil Engineering at Northwestern University and a director of the Center for Advanced Cement-Based Materials. His research interests include constitutive relationships, failure and fracture of concrete, nondestructive testing, and impact and impulsive loading.*

Edward J. Garboczi *is the leader of the Inorganic Building Materials Group in the Building and Fire Research Laboratory at the National Institute of Standards and Technology (NIST). His research interests include modeling the microstructure, transport properties, and mechanical properties of concrete and other random materials.*

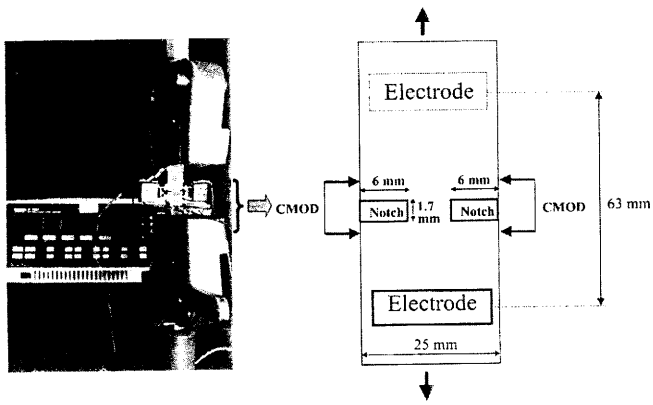

Fig. 1—Test setup.

Sheet specimens were extruded with a 25 mm width and with two different thicknesses, 8 and 4 mm. The specimens were cut to a length of 180 mm to allow sufficient space for electroding, sensing, and gripping for electrical and mechanical tests.

The basic material composition by volume was: 45% cement, 12% silica fume, 1% high-range water-reducing admixture, with a water-binder ratio of 0.25 and silica fume-cement ratio of 0.18. One percent by volume of methylcellulose was added to improve the rheology of the fresh mixture to help the extrusion process. Conductive pitch based carbon fibers were added to the mixture to enhance the electrical properties of the cement composite. Two fiber volume fractions were used: 0.5 and 3%. The fibers were 10 μm in diameter, with a starting length of 25.4 mm (before experiment), having tensile strength of 1770 MPa and modulus of elasticity of 230 GPa. Before extrusion, the liquid phase was mixed together first with the fibers to get a proper dispersion of the fibers in the composite, and then the solid materials were added to the mixture. All the components were mixed together for approximately 10 min until a proper mixture for the extrusion process was achieved.

After extrusion and cutting to final length, the specimens were cured under plastic sheet covers for 1 day and then continued to cure in 100% relative humidity (RH) at room temperature for 14 days. Then the specimens were notched and kept in a constant temperature of 20 C and a constant relative humidity of 50% RH for two days until testing. This was done to stabilize the specimens and to minimize drying effects on the electrical properties during testing.

Test methods

Tensile tests—A closed-loop uniaxial tension test was performed on an MTS machine with a displacement rate of 3×10^{-4} mm/s to characterize the mechanical behavior of the specimens. The specimens were notched 6 mm on each side and tested along the longitudinal direction (that is, the extrusion direction). A gage length of 12.7 mm was employed for controlling the test by using the average of two crack mouth opening displacement (CMOD) gages mounted on each side of the specimen. The setup of the tensile test and the IS measurements is presented in Fig. 1.

Impedance spectroscopy (IS)—The impedance measurements were carried out using a computer-controlled frequency response analyzer over the frequency range of 0.5 to 10^7 Hz (10 points per decade). The excitation amplitude was 1.0 V. The two electrodes were connected on the front and on the back of the specimen with a distance of 63 mm along the length of the specimen, as shown in Fig. 1. The 63 mm distance was measured between the center of the electrodes. The electrodes consisted of copper gauze strips. Paper towel strips were placed between the electrodes and the specimen of the same dimension as the electrodes, 18 x 18 mm, which in turn were in contact with the surface of the specimen. These were held in place with elastic bands. The paper towel strips were saturated with water to facilitate electrochemical contact with the sample. To confirm that test frame interference had been minimized and to provide a baseline for later measurements, specimens were measured prior to mounting and subsequent to mounting, but prior to the application of load.

Digital image correlation (DIC)—DIC was used to monitor the crack growth during the tensile process. DIC is a computer vision technique that compares successive digital images to measure two-dimensional deformation on the surface of the specimen.[11] It is based on tracking a portion of an image (subimage), as the physical feature it depicts moves in a sequence of plane images of a cement surface. This requires a reference image of the unloaded/undeformed specimen, against which subsequent images of the deformed specimen can be compared. This method can be applied during loading, permitting crack growth to be monitored without interfering with the fracture process itself.

Scanning electron microscopy (SEM)—Scanning electron microscopy (SEM) was used to examine the microstructure of polished surfaces of the composites and to characterize the orientation of the fibers in the composite. Fragments of specimens were dried at 60 C and gold-coated for these observations.

Optical microscopy—Optical microscopy was used to examine the length distribution of the fibers in the composite after the mixing and the extrusion process. Representative samples were treated with nitric acid to dissolve away the cement matrix components, leaving the fibers behind. The solution was subsequently sifted through a 75 μm sieve. Images of the remaining fibers left on the sieve were taken with an optical microscope for each specimen. Image analysis was used to measure the final lengths of the fibers in each specimen.

Tested parameters

The main goal of this work was to use the unique electrical properties of conductive fiber-reinforced composites to study the role of fibers in the crack propagation process. For that purpose, the impedance values were measured under tensile loading. Both the mechanical loading and the electrical current were applied along the specimen length, that is, along the extrusion direction. At certain points before and after the peak load, the tensile test was held fixed to enable measurements of the impedance values at relatively constant test conditions (load and displacement). This was done to examine the correlation between crack growth and the electrical impedance of the composite. The development of the crack across the width of the specimen (transverse to the applied load) at each of these points was recorded by a digital camera for subsequent DIC analysis. The impedance values were also measured for unloaded specimens, which were not connected to the MTS testing machine, to give a baseline from which to understand the loaded specimen behavior.

UNLOADED SPECIMENS—ELECTRICAL BEHAVIOR

For unloaded composites, the effects of the following parameters on the impedance values were studied:

Effect of fibers

Presence of fibers—The impedance values were measured for specimens with and without fibers to study the effect of fibers on the electrical behavior.

Fiber orientation—The extrusion process results in a better orientation of the fibers along the extruded direction. The electrical properties were therefore tested along the width (perpendicular to the extrusion direction) and along the length of the specimen (parallel to the extrusion direction), to see any effect on the electrical properties of the composites in each direction.

Fiber content—Specimens with fiber volume fractions of 0.5 and 3% were tested.

Effect of specimen geometry

Specimens with different thickness, 8 and 4 mm, were tested, with the length and width held constant.

The results of the IS measurements on unloaded specimens are presented herein in Nyquist fashion (-imaginary impedance versus real impedance), as in Fig. 2. The Nyquist plot is parameterized by frequency, which decreases from the left (high frequency) to the right (low frequency).

Effect of fibers

Presence of fibers—Figure 2(a) shows the Nyquist plot for a plain cement paste (no fibers) and a 0.5% fiber cement composite. One bulk arc is seen in the case of the plain cement paste (the feature to the right, at low frequency, believed to be associated with surface drying effects), whereas two arcs are apparent in the fiber-reinforced composite spectrum, a low frequency and a high frequency arc. The point where the right side of the low frequency arc touches the real axis is referred to throughout as R_{DC}. This is the true DC resistance of the material, as checked by four-point measurements.[7,8] The cusp between the low and the high frequency bulk arcs of the fiber-reinforced composite is referred to in this paper as R_{cusp}. The dual-arc impedance behavior of short conductive fiber composites was studied by Torrents et al. and is discussed in detail in References 7 and 8. In general, this

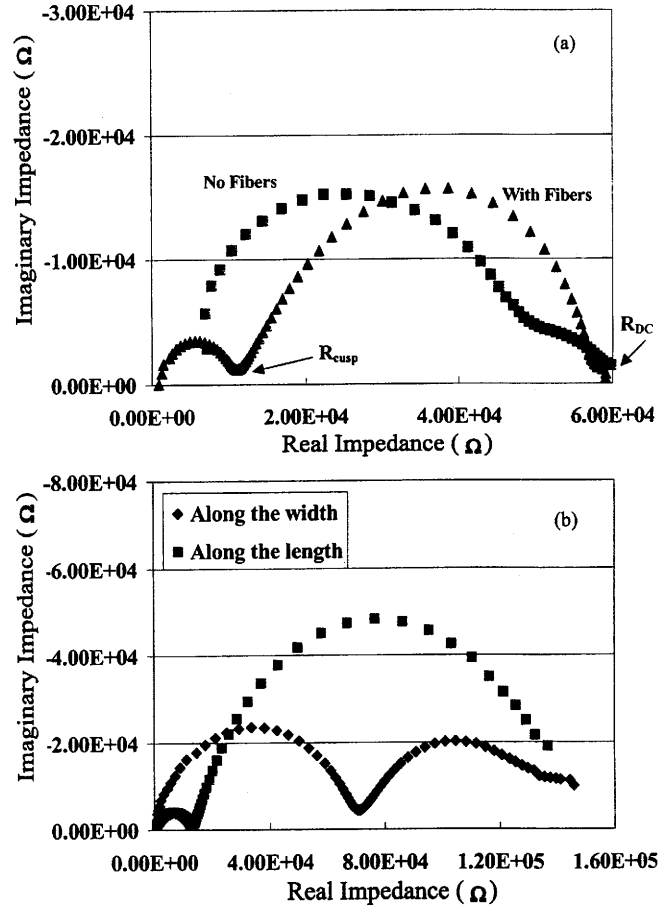

Fig. 2—Effect of fibers on impedance behavior of cement specimen: (a) specimen with and without fibers; and (b) with fibers tested in different directions. (Difference in values between (a) and (b) arises due to difference in geometry [that is, interelectrode spacing] between specimens.)

unique frequency-dependent behavior arises due to highly resistive coatings on the conductive fibers. For steel fibers, this is due to the oxide passivation layer that forms under the high pH pore solution of cement paste. For carbon fibers, a polarization layer (charge transfer resistance/double layer capacitance) forms in the ionic solution of pore fluid. Under DC and low frequency AC excitation, these layers act to make the fibers insulating, so that their effect on the overall electrical transport through the composite is negligible. The value of R_{DC} is therefore almost entirely that of the matrix. As frequency increases, however, the coating impedance goes to zero, causing the fibers to act as short-circuits in the composite. The real resistance of the matrix plus highly conducting fibers is then R_{cusp},[7,8] which is mainly a function of the fibers, not the matrix. In accordance with these ideas, the curves in Fig. 2(a) indicate that the presence of fibers has little or no effect on the value of R_{DC}. The AC behavior, however, is dramatically changed, so that the single bulk arc divides into two separate arcs, giving a value of R_{cusp}.

Fiber orientation—To understand any possible effects of fiber orientation, the impedance values were measured along the width and along the length of the 0.5% fiber composite. The sample was cut to a length of 25 mm, to have similar distances between the electrodes used in both directions. Electrodes with dimensions of 8 x 25 mm were connected to the edges of the specimen in each direction. These kind of electrodes could be used because no loading was applied in

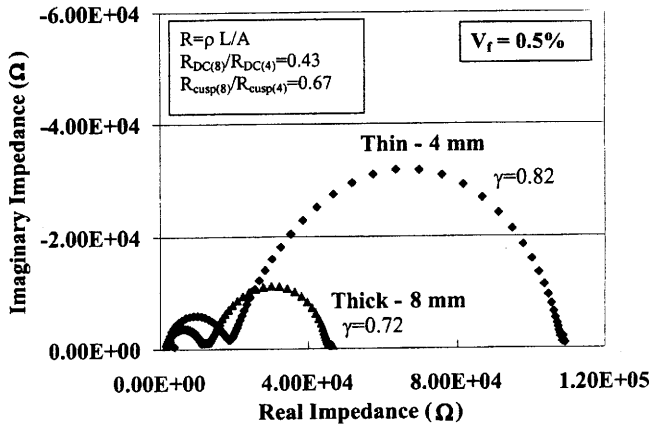

Fig. 3—Impedance behavior of cement composites with different thickness (same length and width).

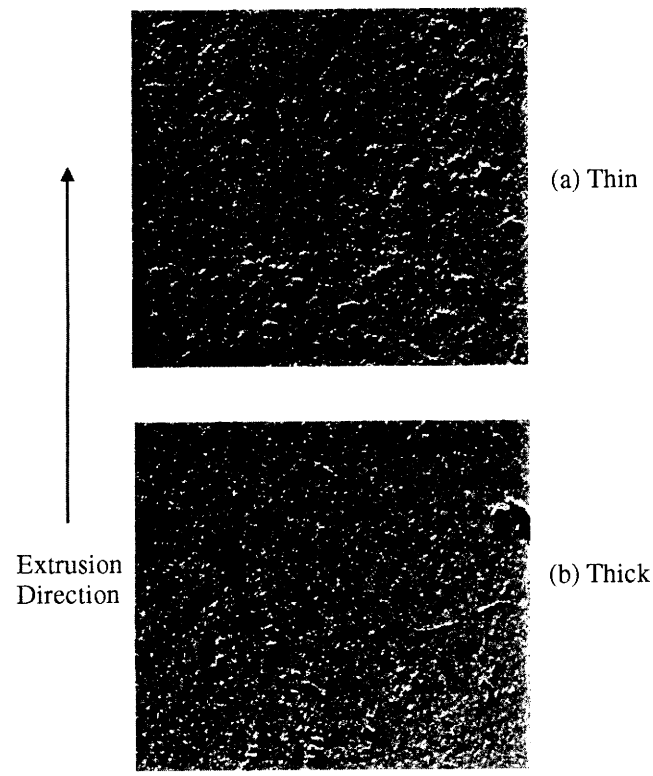

Fig. 4—Scanning electron microscope (SEM) micrograph of cement composite with different thickness: (a) 4 mm; and (b) 8 mm.

this case. Figure 2(b) presents the impedance behavior of the specimen in both directions. There is little or no difference between the R_{DC} values in both directions, which is expected, as the R_{DC} value depends mainly on the matrix, which is not much affected by the extrusion process.

The R_{cusp} values in Fig. 2(b), however, are dramatically changed, with the resistance at the cusp much greater for the impedance measured along the width of the specimen (perpendicular to the extrusion direction). The samples were produced with the extrusion process, which causes the fibers to be relatively oriented along the specimen length, that is, along the direction of the extrusion process.[12] Therefore, the lower value of R_{cusp} at high frequency for the impedance measurement along the length can be related to the greater fiber orientation in this direction.

Fiber orientation along the current can be characterized by the γ parameter, which is the ratio between the low frequency arc diameter to the DC resistance

$$\gamma = (R_{DC} - R_{cusp})/R_{DC} \quad (1)$$

Greater fiber orientation results in higher values of γ.[7,13] Herein, for samples tested along the width of the specimen (perpendicular to the extrusion direction), the value of γ is relatively low, 0.54. In extruded composites, there is some orientation of fibers along the width of the specimen, giving a nonzero value of γ in this direction. The value of γ, however, is enhanced to a value of 0.91 along the direction of the extrusion process due to better orientation of the fibers in this direction. Again note that the values of R_{DC} observed in the different tested directions clearly show that the DC conductivity was not affected by the fibers, while the values of R_{cusp} clearly were. Similar dependence on fiber orientation was previously observed on similar specimens.[7]

Effect of specimen geometry

The total electrical resistance of an un-notched sample R measured along the extrusion direction is dependent on the cross-sectional area of the specimen that can transfer current

$$R = \rho L/A \quad (2)$$

where

A = transfer area of the current;
ρ = electrical resistivity of the matrix; and
L = distance between the electrodes.

Increasing the cross-sectional area A leads to a reduction in the resistance of the composite. This trend is clearly observed in Fig. 3, which shows the impedance response of two cement composites with different thicknesses, 8 and 4 mm. The 25 mm length and 63 mm width of these composites were the same, and both specimens were extruded from the same batch of cement and carbon fibers. Based on Eq. (2), it is expected that the ratio between the R_{DC} values of these composites (8/4 mm), as well as the ratio between their R_{cusp} values, will be equal to the ratio of their cross-sectional areas, which, in this case, is 0.5. The actual ratio between the R_{DC} values of these two composites is 0.43, which is close to the expected value of 0.5 but not equal, due to the inhomogeneity of these specimens. The ratio, however, between the R_{cusp} values of these composites is quite different, 0.67. The values of γ are also not the same: γ = 0.82 for the 4 mm specimen, compared to γ = 0.72 for the 8 mm thick specimen. This difference suggests that there must be a difference in fiber orientation between the two systems. Such a difference was also observed under SEM, as seen in Fig. 4, which shows polished sections of both composites. In the thin specimen, better alignment of the fibers can be seen along the extrusion direction, that is, in the direction of applied current. Forcing the composite material through a thinner die opening in the extrusion process results in a greater degree of orientation, thus at least partially explaining the higher ratio of 0.67 between the R_{cusp} values of these two composites compared to the expected ratio of 0.5. This indicates once again the sensitivity of R_{cusp} to the presence of fibers and their arrangement in the composite.

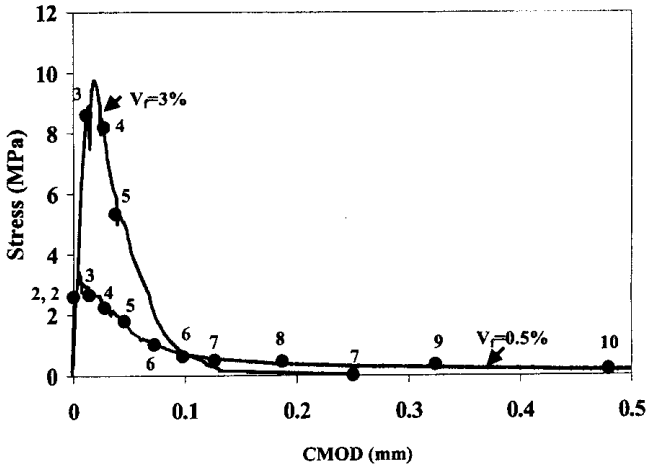

Fig. 5—Tensile behavior of cement composites with volume fraction of 0.5 and 3%.

EXPERIMENTAL UNCERTAINTIES

The experimental uncertainties in load and CMOD measurements at peak are estimated to be ±12 and 10%, respectively. The absolute uncertainty in electrical resistance values (R_{DC}, R_{cusp}) derived from impedance measurements is estimated to be ±5 to 10%. This arises from variability in electrode geometry (for example, contact area, interelectrode spacing). In the case of the crack opening experiments, where electrode geometry remains roughly constant during the course of experiments, relative uncertainty will be much smaller, for example, less than ±1%.

ELECTRICAL AND MECHANICAL BEHAVIOR UNDER LOADING

Based on the previous observations, the sensitivity of the R_{DC} values to changes in the cement matrix and the sensitivity of the R_{cusp} values to a change in the fibers was also expected to appear during loading. More precisely, any changes in the matrix due to cracking will affect both R_{DC} and R_{cusp}, while any changes in the fibers will mainly affect R_{cusp}. Correlating the fracture process and the impedance values should aid in understanding the composite fracture behavior.

Mechanical behavior

Figure 5 presents the tensile response of 0.5 and 3% fiber composites. The points labeled on the curves represent the stages where the displacement was temporarily held to measure the impedance values and perform DIC. The tensile stresses were calculated based on the net area between the notches. It is clear from Fig. 5 that the composite with the larger content of fiber (3%), is stronger and tougher than that with the lower content of fiber (0.5%), as expected. It can also be seen that the 3% fiber composite fully fractured at a lower CMOD (approximately 0.25 mm) than did the 0.5% fiber specimen (approximately 0.5 mm). While the tensile peak is more sensitive to the number of fibers present, the width of the tail is more sensitive to fiber length. Thus, Fig. 5 gives some indication that the fibers in the 0.5% specimen were longer than those in the 3% specimen, a point that will be discussed more extensively to follow.

Impedance behavior

The impedance responses of the 0.5% fiber composite during the fracture process are presented in Fig. 6, for the entire

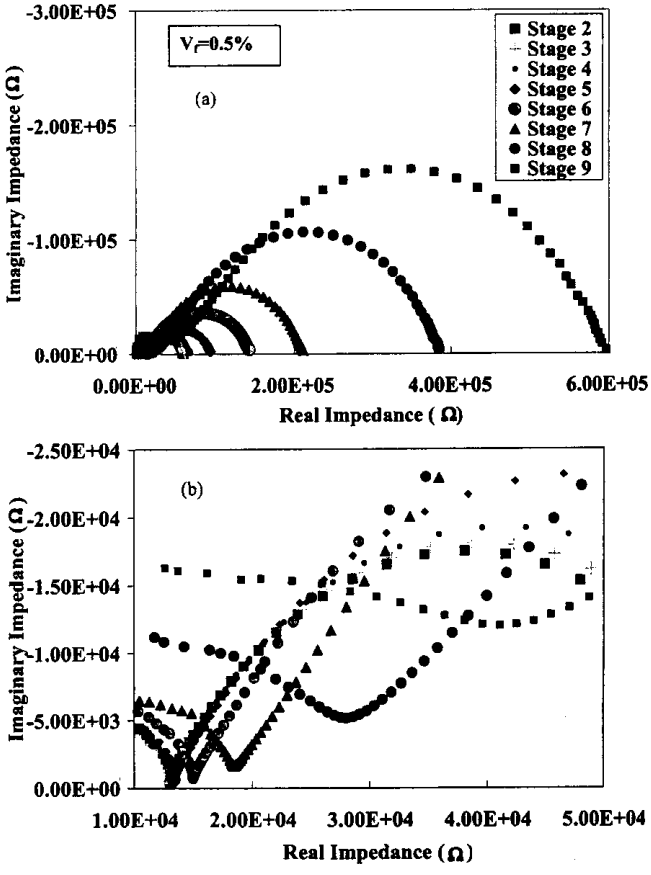

Fig. 6—Impedance behavior of cement composites with volume fraction of 0.5%: (a) full scale (R_{DC} values); and (b) blow-up of high frequency arcs (R_{cusp} values).

frequency range (Fig. 6(a), showing the R_{DC} values) and for the high frequency arcs only (Fig. 6(b), showing the R_{cusp} values). The numbered stages are the same as those labeled in Fig. 5. Figure 6 shows the correlation between the fracture process and the impedance values, for both the R_{DC} and the R_{cusp} values. The electrical resistance of the composite increases through the fracture process. As the crack propagates, the current is progressively restricted to a smaller and smaller cross-sectional area of the composite, leading to an increase in both R_{DC} and R_{cusp}. Similar behavior of the impedance during the fracture process was also observed for the 3% fiber composite. The increase in the composite resistance through the development of the crack is evident in Fig. 7, which shows the impedance values, R_{DC} and R_{cusp}, versus CMOD for both fiber contents. The trend is similar for both systems for both impedance values: greater CMOD results in higher resistance. The relationships between the impedance values and the CMOD for each system, however, is different. For the 0.5% fiber composite, as the fracture process initiates, the R_{DC} values increase gradually with crack growth, while at the same time there is no significant increase in the R_{cusp} values. Only for higher values of CMOD do the R_{cusp} values start increasing. For the 3% fiber system, the behavior of the impedance values is rather different. Both R_{DC} and R_{cusp} hardly change at low CMOD, but then a sudden increase is observed at larger values of CMOD. A comparison between the R_{DC} values of both systems at low CMOD clearly shows this differing behavior, as presented in Fig. 8.

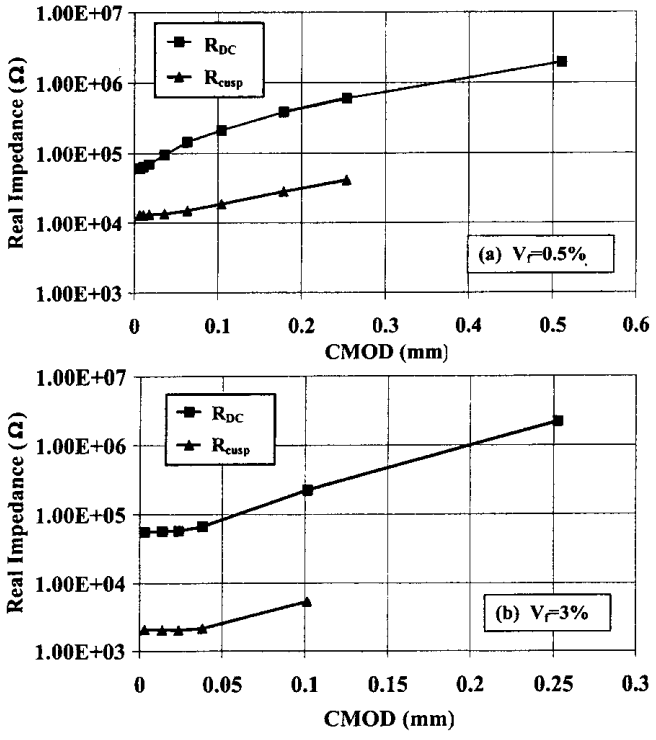

Fig. 7—R_{DC} and R_{cusp} values versus crack opening of cement composite with: (a) 0.5%; and (b) 3%, by volume, fibers.

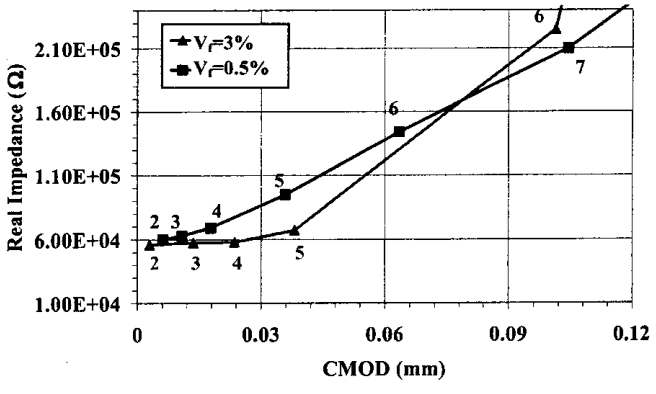

Fig. 8—Impedance values R_{DC} versus crack mouth opening displacement (CMOD) of composites with volume fraction of 0.5 and 3%.

There are two possible explanations for the different impedance behavior between the two composites during fracture. First, underlying differences in the overall composite microstructure could lead to differing current distributions and electrical behavior under load and in the presence of growing cracks. For example, differences in fiber/matrix bonding, matrix porosity, fiber length, and fiber alignment could result in completely different responses during crack propagation. An indication of such differences in behavior can be seen in the electrical properties of the unloaded composites. Their longitudinal DC resistances differed by a factor of 1.5 (3.9×10^4 ohms for the 3% fiber specimen versus 6.1×10^4 ohms for the 0.5% fiber specimen), but their corresponding cusp resistances differed by as much as a factor of 6 (2.0×10^3 ohms for the 3% fiber specimen versus 1.2×10^4 ohms for the 0.5% fiber specimen).

The second explanation for the differing impedance behavior between the composites in Fig. 8 has to do with local

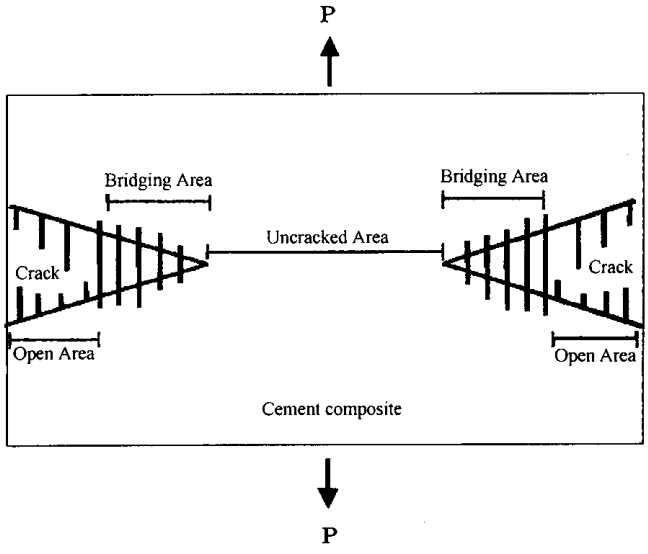

Fig. 9—Different areas across current flow during fracture process.

microstructural effects along the crack front. As the crack propagates during loading, three different areas can be distinguished in the composite cross section between the notches in Fig. 1. Figure 9 shows a schematic representation of these areas: 1) the open area; 2) the uncracked area; and 3) the bridging area.

The open area (1) is the portion of the cross section of the composite where the crack has propagated and there is no remaining fiber connection. Herein, the matrix is fractured and the fibers are either fractured or fully pulled-out. In this case, current cannot be transferred across the crack, because neither the cement paste matrix nor the fibers are connected;

The uncracked area (2) is the portion of the sample cross section where the propagating crack has not yet reached. Herein, the transport of the current at low frequency is through the uncracked matrix and at high frequency through the fibers in the matrix. Reduction in this area increases both R_{cusp} and the R_{DC}; and

The bridging area (3) is the part of the cross section of the composite where the matrix is fractured but there is still fiber bridging. The extent of the bridging area is dependent on the fiber failure mechanism, for example, fracture and/or pull-out, and the embedded length of these fibers. These bridging fibers can transfer current across the crack front at high frequency, thereby affecting the value of R_{cusp}, but cannot transfer current at low frequency, due to the high resistance coating between the fibers and the cement matrix. Therefore, as far as the value of R_{DC} is concerned, Areas (1) and (3) are equivalent.

The different ways in which R_{DC} and R_{cusp} react to the three areas allows one to use the electrical impedance signal to analyze the mechanical information and identify these areas as a function of CMOD. Quantitative description of these areas at different loading stages for different composite systems can result in better understanding of the microstructure-mechanical property relationships of cement composites during the fracture process and the role of fibers during this process. It should be stressed that the model in Fig. 9 assumes a planar crack front, which is certainly not obtained in practice (see as follows). Nevertheless, this equivalent planar transfer area approach can provide useful insight about the fracture mechanics of fiber-reinforced composites.

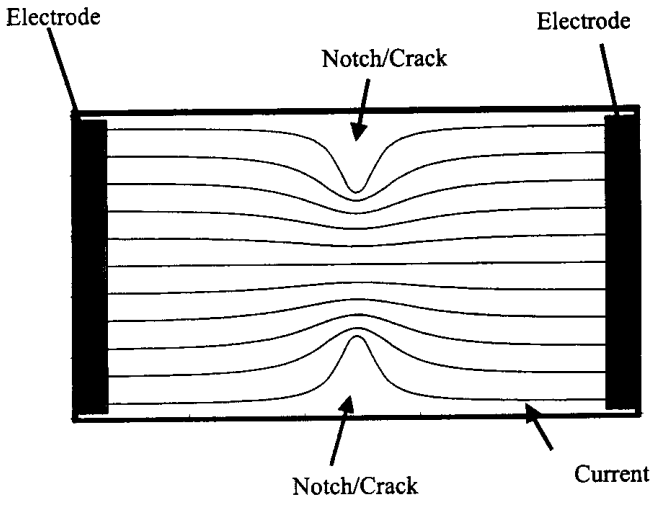

Fig. 10—Schematic description of current behavior in cracked/notched specimen.

Physical and computer simulations

Two techniques were used to calculate the different areas: empirical and analytical. Essentially what is needed to be known is how R_{DC} and R_{cusp} depend on the cross-sectional area available for current flow.

Empirical method—Cement composites with both fiber contents were notched on both sides of the specimen at different notch lengths: 0 (no notch), 3, 6, 9, and 11 mm. The 11 mm notch length was possible only for the 3% fiber composites. The impedance values were measured for unloaded specimens and plotted, for each notch length, versus the transfer area (that is, the unnotched area). This procedure controls the crack length and the transfer area of the current through the unnotched region. Note that herein the crack (notch) is applied through all the specimen thickness, and that there is no bridging area due to fibers. In this test, the distance between the electrodes was 50 mm and the notch lengths were progressively increased on the same specimen after each impedance measurement.

Numerical simulation method—The current behavior is not linear in a cracked/notched composite, as presented in Fig. 10, and the geometry, though simple, does not lend itself to easy analytical calculation. Therefore, a finite element analysis was used to calculate the impedance values for different notch lengths. For that purpose, a FORTRAN 77 program was used to carry out a pixel-based computation.[14] This and similar programs were designed to compute the electrical and elastic properties of random materials whose microstructure can be represented by a three-dimensional digital image. They can also be used to simulate nonrandom, but analytically intractable geometries, as in the present study. The program is a finite element program, for use in DC problems only.

Pixels in a three-dimensional digital image were used to construct a digital image representation of the samples and electrodes used in the laboratory studies. The length scale used was 1/3 mm/pixel. Enough pixels were used to match the overall sample dimensions (extra air pixels were taken on the outside of the image to turn off the periodic boundary conditions that are built into the program[14]). Each pixel in the simulated structure is taken to be a trilinear finite element, where Laplace's equation was set up and solved in a variational form. A phase label (1,2,3,...) is given to each

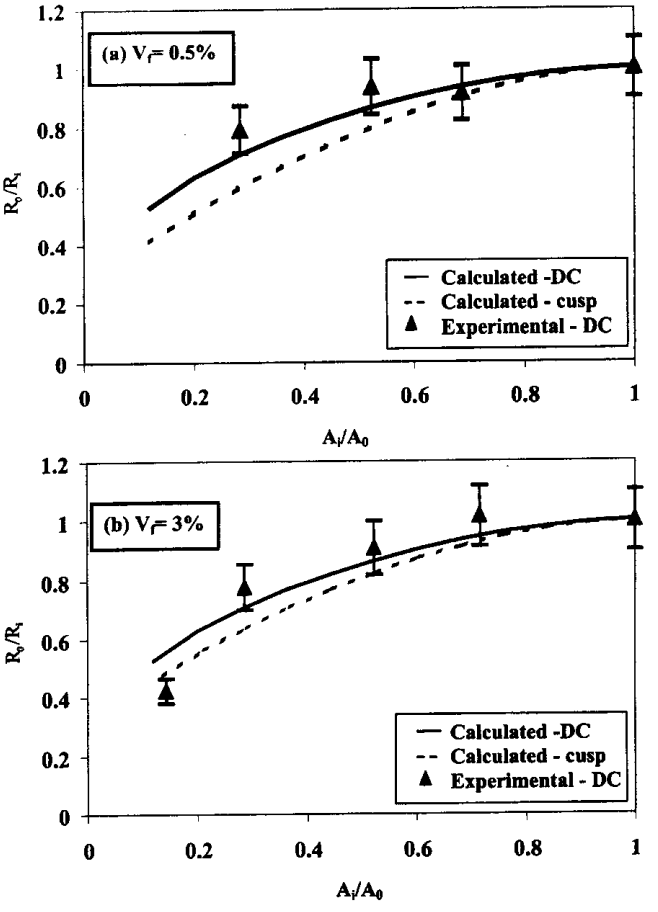

Fig. 11—Calibration curves for calculating different areas on notched experiment and finite element analysis: (a) 0.5% fiber content; and (b) 3% fiber content.

pixel, denoting which material phase is in that pixel. The full (symmetric) conductivity tensor is used in each phase, and can be different for different phases. The notches were taken to be 1.67 mm wide, and 0, 3, 6, 9, and 11 mm long, almost exactly matching the experimental quantities. Once the image of the sample was set up in the program, conductivity tensors were assigned. The conductivity tensor in the fiber-reinforced material had the measured anisotropic, diagonal conductivity tensor, where (σ_x, σ_y, σ_z) = (1, 1.1, 0.68), (1, 0.2, 0.2), (1, 0.99, 0.47), and (1, 0.21, 0.12) for 0.5% DC, 0.5% cusp, 3% DC, and 3% cusp, respectively, in arbitrary units. Arbitrary units could be used, as all results are normalized by the values for the zero-notch situation in each case. The electrodes were taken to be in exactly the positions that they were in the experiment, with the voltage of one electrode set to a 1 v, and the other to 0 v.

Figure 11(a) and (b) show the results of the simulated crack (notch) studies for the 0.5 and 3% fiber specimens, respectively. In each case, the R_{DC} and R_{cusp} values are normalized by the corresponding resistances of the un-notched specimen, and the remaining area between the notches has been normalized by the cross-sectional area of the un-notched specimen. In each diagram, the solid line corresponds to the finite element analysis results for R_{DC} versus transfer area, and the dashed line corresponds to the finite element analysis results for R_{cusp} versus transfer area curve (all suitably normalized). Also plotted are actual R_{DC} data for notched composites. Between successive data

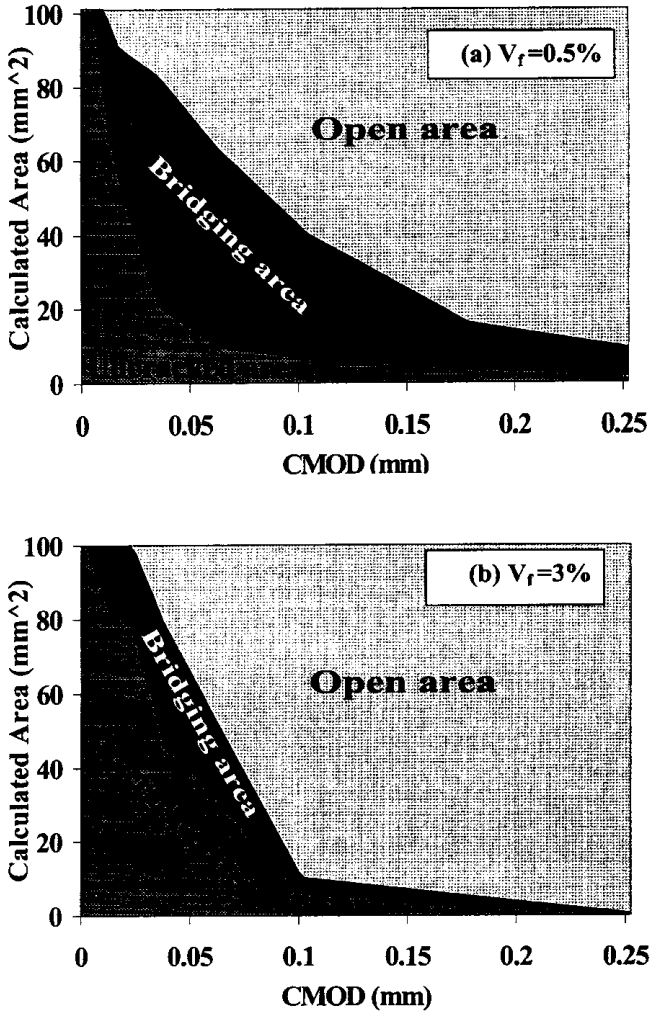

Fig. 12—Calculated areas versus crack opening for different composites: (a) 0.5% fibers by volume; and (b) 3% fibers by volume.

points, the electrodes were removed, the sample was more deeply notched, and the electrodes were reapplied. The ±10% error bars, as shown, are therefore appropriate. Note that the datum for the smallest remaining area falls significantly below the finite element analysis line in the case of the 3% fiber system. At this point, the notch depth was 11 mm, leaving only 3 mm of material between the notches. It is suspected that damage in this un-notched region results in anomalously low conductance (higher R_{DC}). At the same notch length, the 0.5% fiber specimen failed altogether and therefore could not be measured. Otherwise, there is good agreement between the experimental and calculated R_{DC} versus transfer area results. Experimental R_{cusp} measurements were also made, but these data tended not to be reproducible from sample to sample, and their scatter was quite large. The trend of the R_{cusp} values versus transfer area was roughly the same as that of R_{DC} in Fig. 11(a) and (b).

The fact that there is little difference in the transfer area-dependence of R_{DC} and R_{cusp} between the 0.5% fiber and 3% fiber composites in Fig. 11 suggests that global differences in microstructure/electrical response between the two composites is not responsible for their differing impedance behavior during crack growth (Fig. 8). Rather, local microstructural differences along the crack front must account for the differences.

Transfer area analysis

The computed curves in Fig. 11(a) and (b) were used as calibration curves to obtained the associated current transfer areas from the data in Fig. 7 and 8. The area calculated from the R_{DC} values is the uncracked area, while the area calculated from R_{cusp} is the uncracked plus bridged area. The difference of these two areas is therefore the fiber bridging area. These areas for both composite systems, 0.5 and 3% by volume of fibers, are presented in Fig. 12(a) and (b), respectively.

There are clear differences in behavior between the two composites. At any given CMOD beyond 0.04 mm, the bridging area is noticeably larger for the low fiber content composite. The maximum bridging area for the 0.5% fiber composite is nearly 60% at 0.03 mm CMOD versus 20% for the 3% fiber composite. At the same CMOD (0.03 mm), the uncracked area is significantly less in the 0.5% fiber composite (≈20%) than in the 3% fiber composite (≈50%). Another way to view this is that overall crack propagation (open plus bridged areas) is less for the higher fiber content, as would be expected based upon the overall mechanical properties in Fig. 5. What is surprising is the persistence of fiber bridging in the low fiber content composite, out to a CMOD of 0.25 mm. In contrast, the bridging area drops precipitously for the 3% fiber composite after the onset of fiber failure at 0.025 mm CMOD, whereafter it closely tracks the overall crack front (the boundary between the bridging area and the uncracked area). Beyond 0.1 mm CMOD, little or no bridging area is observed.

Crack development

Observations on the crack growth during loading of both composites are seen in Fig. 13. These images were calculated based on the DIC technique, as previously mentioned, and were taken during the holds in the loading process at each impedance measurement. Prior to Stage 6, the development of the crack for the 3% fiber system is relatively small. A significant increase in crack growth from Stage 5 to 6, however, is evident for this system. A sudden change from Stage 5 to 6 also appears in the impedance values of this system (Fig. 8). On the other hand, in the 0.5% fiber composite, the crack initiates and develops more gradually throughout the fracture process (Fig. 13). This behavior of the crack correlates with the gradual change in the impedance values measured during the fracture process (Fig. 8). There is a good general correlation between the impedance values and the fracture process, as well as the more detailed analysis of the bridging area available from the impedance measurements. Thus, the differences in the calculated areas of the two fiber content systems previously discussed (Fig. 12) are a result of differences in crack development in each system.

A delay in the propagation of the crack is expected when a sufficient volume of microfibers are used.[15] Uniformly dispersed microfibers can suppress growth of microcracks and enhance tensile strength of the composites. Such a delay in crack propagation, along with a small change in the impedance values (both R_{DC} and R_{cusp}) up to Stage 5, were seen with the 3% fiber system (Fig. 13, 7, and 8). This delay in crack propagation may explain the greater uncracked area in the 3% fiber system compared with a smaller uncracked area in the 0.5% fiber system, at low CMOD, up to approximately 0.1 mm (Fig. 12). The lower fiber content composite had a more steady, but gradual, crack development from initiation onwards. Nevertheless, this delay in crack propagation for the 3% fiber material does not explain the greater bridging area of the 0.5% fiber

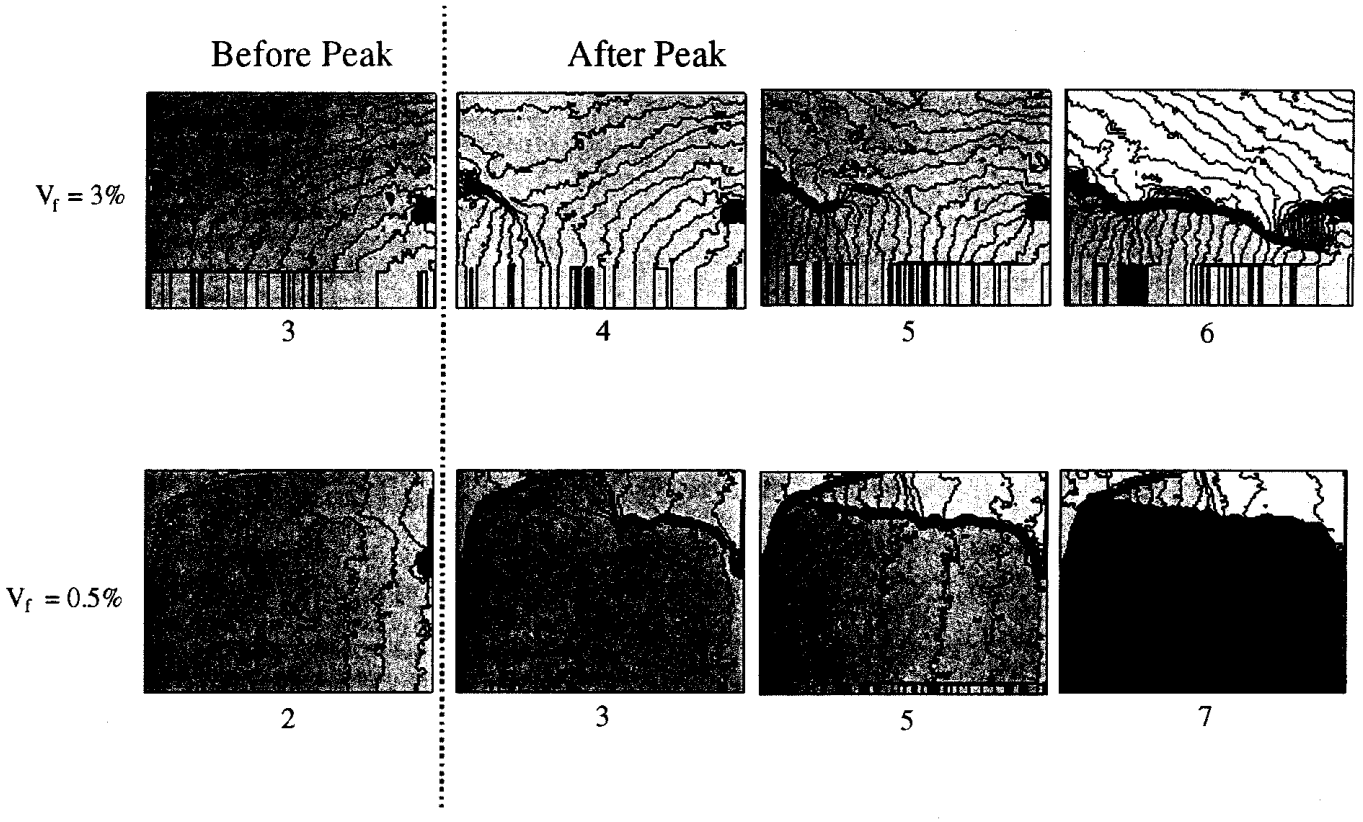

Fig. 13—Crack propagation for composites with different fiber contents. Numbers correspond to different stages during testing.

system compared with that of the 3% fiber system, from 0.04 mm and larger CMOD. Despite the low amount of fibers, a larger cracked area is bridged by the fibers (at higher CMOD). To understand this phenomenon, fiber length in the two composites was investigated by optical microscopy.

Extrusion pressure and fiber length

Carbon fibers are quite brittle. It was reported that such fibers tend to break during mixing.[2,3] It should be kept in mind that in this work, the cement composites were produced by extrusion. In this process, the fresh mixture is relatively stiff (water-binder ratio of 0.25 in this case). Such a stiff mixture requires high forces during mixing and extruding. Increasing the content of the fibers in the mixture requires even greater forces for mixing and extrusion. It is likely that these high forces will break the brittle carbon fibers during mixing and extruding. One way to evaluate the rheological properties of a stiff mixture is by measuring the pressure applied during the extrusion process. A stiffer mixture results in higher pressure required for the extrusion process. Herein, the pressure needed to extrude the 0.5% fiber specimens was 11.3 versus 37.6 MPa for the 3% fiber composite (at the same extrusion rate). Such high stresses can significantly damage the carbon fibers and reduce their length.

The final length of the fibers after the extrusion process in each composite system was examined by optical image analysis of the remains of nitric acid dissolution of the composite matrices. Image analysis was used to measure the length distribution of the remaining fibers. The results are presented in Fig. 14, which shows the normalized cumulative distribution of fiber length for both fiber systems. It can be seen, for example, that in the 3% fiber system, approximately 55% of the fibers are less than or equal to a length of 0.5 mm, whereas in the 0.5% fiber system only 30% of the fibers are below this

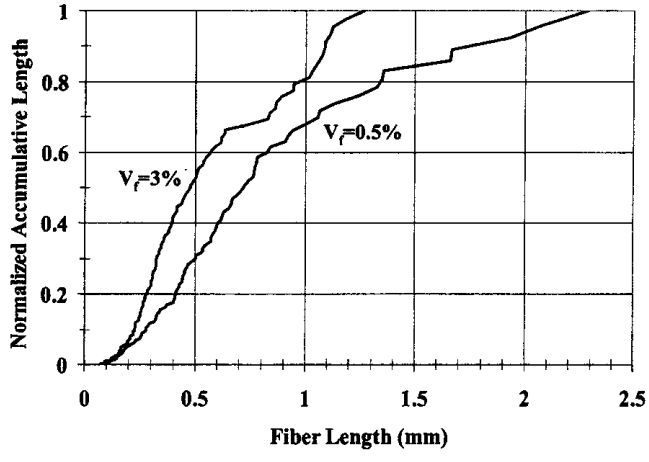

Fig. 14—Length distribution of fibers in different cement composites with volume fraction of 0.5 and 3%.

length. In addition, the maximum length of the fibers in the 0.5% fiber composite is greater, by a factor of approximately 2, than the maximum length of the fibers in the 3% composite. It can be concluded that the fibers are shorter in the 3% fiber composite than in the 0.5% fiber composite, undoubtedly due to the higher forces and pressure needed to mix and extrude the stiff 3% fiber mixture, as previously discussed. Shorter fibers reduce the potential displacement of the fibers bridging the crack, when these fibers are completely pulled-out from the matrix, leading to a low strain capacity of the composite.[3] The shorter fibers in the 3% fiber composite lead to complete fracture at a small CMOD of only 0.25 mm, compared with the larger CMOD of 0.5 mm required for full fracture of the 0.5% fiber composite (Fig. 5). Shorter fibers

ture, and CH/ash ratio. The results, shown in Table 5, illustrate that while the pH does evolve with time and is a function of temperature, the pH does not change as a function of CH/ash ratio, and thus it is safe to assume that the pH of the system is set by the pH of the NaOH solution.

Finally, Taylor and Turner, and Beaudoin et al. suggest that the use of methanol to quench hydration may cause undesirable interactions when using TGA to quantify residual CH.[28,35] This, however, is particularly the case when quantifying small amounts of CH hydration byproduct. To demonstrate that the use of methanol had no significant effect in the present experiments, TGA data for as received CH and methanol washed CH were compared. No differences were noted.

SUMMARY OF RESULTS

A method for determining the apparent activation energy for the pozzolanic reaction of low CaO containing fly ash is suggested. The technique involves reacting CH/ash pastes in simulated pore solution at fixed temperatures and times. The apparent activation energy for CH consumption is on the order of 69 kJ/g-mol. All experiments were conducted in a pH 13.4 NaOH solution. Preliminary data suggests that the stoichiometry of the hydrate phase depends upon the CH/ash ratio and that the rate of CH disappearance and the rate of hydrate formation is a function of CH content. Considerable work is yet required to describe these observations with mechanistic arguments. Microstructural data, as well as more detailed XRD and calorimetric studies, are suggested.

A single fly ash was investigated by reaction in pH 13.4 NaOH solution to mimic pore solution pH at later stages of hydration, as noted by other investigators. Similar studies should be conducted in the absence of NaOH (pH approximately 12.7 for CH) and at other pH values and with other cation and anions present in solution, that is, K^+ and SO_4^{-2}. Ashes with various amounts of aluminate and CaO phases should then be studied to understand the effect of chemical composition on reactivity. Finally, comparison of model-predicted performance and performance in portland cement systems would be useful.

ACKNOWLEDGMENTS

The authors would like to acknowledge the financial support of Holnam, Inc. A special thank you is also extended to Geoffrey Frohnsdorff of the Building Materials Division of the National Institute of Standards and Technology (NIST) for being host to the senior author during the summer of 1998, when the majority of this research was conducted.

REFERENCES

1. Bentz, D. P., "A Three-Dimensional Cement Hydration and Microstructure Program—I: Hydration Rate, Heat of Hydration, and Chemical Shrinkage," *National Institute of Standards and Technology BFRI*, MISTIR 5756, 1995.

2. Bentz, D. P., and Remond, S. "Incorporation of Fly Ash into a 3-D Cement Hydration Microstructure Model," *National Institute of Standards and Technology BFRI*, NISTIR 6050, Aug. 1997.

3. Jensen, O. M., "The Pozzolanic Reaction of Silica Fume," TR 229.90, Building Materials Laboratory, Technical University of Denmark, 1990. (in Danish)

4. Bentz, D. P.; Waller, V.; and De Larrard, F., "Prediction of Adiabatic Temperature Rise in Conventional and High-Performance Concretes Using a 3-D Microstructural Model," *Cement and Concrete Research*, V. 28, No. 2, 1998, pp. 285-297.

5. Helmuth, R., *Fly Ash in Cement and Concrete*, Portland Cement Association, 1987, pp. 203.

6. "Blended and Modified Cements," P. W. Brown, ed., *Cements Research Progress* (1989-1990), L. Struble, ed., *Cements Research Progress*, American Ceramic Society (1993-1997).

7. Ma, W.; Sample, D.; Martin, R.; and Brown, P. W., "Calorimetric Study of Cement Blends Containing Fly Ash, Silica Fume and Slag at Elevated Temperatures," *Cement and Concrete Aggregates*, V. 16, No. 2, Dec. 1994.

8. Takemoto, K., and Uchikawa, H., "Hydration of Pozzolanic Cement," *7th International Congress on the Chemistry of Cement*, V. I, 1980, 2/1-2/29.

9. Fajun, W.; Grutzeck, M. W.; and Roy, D. M., "The Retarding Effects of Fly Ash upon the Hydration of Cement Pastes: The First 24 Hours," *Cement and Concrete Research*, V. 15, 1985, pp. 174-184.

10. Yamazaki, K., "Fundamental Studies of Effects of Mineral Fines on Workability of Concrete," *Transactions of the Japan Society of Civil Engineers*, V. 84, 1962, pp. 98-118; V. 85. pp. 15-44. (in Japanese)

11. Helmuth, R., *Fly Ash in Cement and Concrete*, Portland Cement Association, 1987, 110 pp.

12. Lilkov, V.; Dimitrovan, E.; and Petrov, O. E., "Hydration Process of Cement Containing Fly Ash and Silica Fume: The First 24 Hours," *Cement and Concrete Research*, V. 27, No. 4, 1997, pp. 577-588.

13. Fajun, W.; Grutzeck, M. W.; and Roy, D. M., "The Retarding Effects of Fly Ash upon the Hydration of Cement Pastes: The First 24 Hours," *Cement and Concrete Research*, V. 15, 1985, pp. 174-184.

14. Ogawa, K.; Uchikawa, H.; Takemoto, K.; and Yasui, I.,"The Mechanism of the Hydration in the System C3S-Pozzolana," *Cement and Concrete Research*, V. 10, 1980, pp. 683-696.

15. Shi, C., "Early Microstructure Development of Activated Lime-Fly Ash Pastes," *Cement and Concrete Research*, V. 25, No. 9, 1996, pp. 1351-1359.

16. Shi, C., "Pozzolanic Reaction and Microstructure of Chemical Activated Lime-Fly Ash Pastes," *ACI Materials Journal*, V. 95, No. 5, Sept.-Oct. 1998, pp. 537-545.

17. Katz, A., "Microscopic Study of Alkali-Activated Fly Ash," *Cement and Concrete Research*, V. 28, No. 2, 1998, pp. 197-208.

18. *Ash Production Ash Utilization—1984*, American Coal Ash Association, Aug. 1, 1985, Washington, D.C.

19. Taylor, H. F. W.; Mohan, M.; and Moir, "Analytical Study of Pure and Extended Portland Cement," *Journal of the American Ceramics Society*, V. 68, No. 12, 1985, pp. 685-690.

20. ASTM C 311, "Standard Test Methods for Sampling and Testing Fly Ash or Natural Pozzolans for Use as a Mineral Admixture in Portland-Cement Concrete," *Annual Book of ASTM Standards*, V. 4.02, West Cohshohocken, Pa., 1986, pp. 236-243.

21. Thorne, D. J., and Watt, J. D., "Composition and Pozzolanic Properties of Pulverized Fuel Ashes—II: Pozzolanic Properties of Fly Ashes, as Determined by Crushing Strength Testis on Lime Mortars," *Journal of Applied Chemistry*, V. 15, 1965, pp. 595-604.

22. Watt, J. D., and Thorne, D. J., "The Composition and Pozzolanic Properties of Pulverized Fuel Ashes—III: Pozzolanic Properties of Fly Ashes and Determined by Chemical Methods," *Journal of Applied Chemistry*, V. 16, 1966, pp. 22-29.

23. Minnick, L. J., "Fundamental Characteristics of Pulverized Coal Fly Ashes," *Proceedings*, ASTM, V. 59, 1959, pp. 1155-1177.

24. Joshi, R. C., and Rosauer, E. A., "Pozzolanic Activity in Synthetic Fly Ashes—I: Experimental Production and Characterization," *American Society of Ceramics Bulletin*, V. 52, No. 5, 1973, pp. 456-458.

25. Fraay, A. L. A.; Bijin, J. M.; and de Haan, Y. M.,"The Reaction of Fly Ash in Concrete: A Critical Examination," *Cement and Concrete Research*, V. 19, 1989, pp. 235-246.

26. Hobbs, S. V., "Degree of Hydration Procedure," *National Institute of Standards and Technology BFRL*, Building Materials Division, Aug. 1997.

27. Minor, D., "Ash Characterization Reports, Surface Areas and Particle Size Distributions, Samples No. 9701, 9702, 9703, 9704 and Ca(OH)2," National Institute of Standards and Technology Powder Characterization Laboratory, June 1998.

28. Taylor, H. F. W., and Turner, A. B., "Reactions of Tricalcium Silicate Paste with Organic Liquids," *Cement and Concrete Research*, V. 17, No. 4, pp. 613-623.

29. Williams, P. J.; and Biernacki, J. J.; Walker, L. R.; Meyer, H. M.; Rawn, C. J., "Microanalysis of Alkali Activated Fly Ash/CH Pastes." (in progress)

30. Avrami, M., "Kinetics of Phase Change—I," *Journal of Chemical Physics*, V. 7, 1939, pp. 1103-1112.

31. Knudsen, T., "The Dispersion Model for Hydration of Portland Cement," *Cement and Concrete Research*, V. 14, 1984, pp. 622-630.

32. Brown, P. W.; Pommersheim, J. M.; and Frohnsdorff, G., "Kinetic Modeling of Hydration Processes," *Cement Research Progress*, 1979, American Ceramics Society, Ohio, 1979, pp. 246-260.

33. Dolch, W. L., "Evaluation of Methods of Identifying Phases of Cement Paste," *Transportation Research Circular* No. 176, Transportation Research Board, Washington D.C., June 1976.

34. Young, J. F., and Hansen, W., *Materials Research Society Symposium Proceedings*, V. 85, 1987, pp. 313.

35. Beaudoin, J. J.; Gu, P.; Marchand, J.; Tamtsia, B.; Myers, R. E.; and Liu, Z., "Solvent Replacement Studies of Hydrated Portland Cement Systems: The Role of Calcium Hydroxide," *Advanced Cement-Based Materials*, V. 8, No. 2, 1998, pp. 56-65.